

HELICOPTER ENGINE INTAKE BARRIER FILTER DESIGN

Nicholas Bojdo¹ & Antonio Filippone
The University of Manchester
Manchester M60 1QD
United Kingdom

ABSTRACT

This contribution concerns the design of Intake Barrier Filters (IBF) for Helicopters. These protective devices are fitted to the engine intakes of helicopters to prevent sand and dust reaching the engine during operations in dusty environments. Their design is dependent on and unique to the rotorcraft to which they are fitted, and can be optimised for minimum pressure drop and maximum service life accordingly by tuning the filter geometry. Three main constraints govern the design of IBF. They are: 1) Intake architecture; 2) Engine mass flow; 3) Particle size distribution of local dust. The filter is a pleated multi-ply fabric. By changing the fold depth and pitch, the filter can be optimised to perform at minimum pressure drop and maximum particle capture capacity for a given constraint set. It is found that the latter of these favours fifty percent more filter folds for optimum performance.

KEYWORDS: Inlet barrier filter, pleated filter, intake devices, helicopter engine installation losses.

INTRODUCTION

Helicopters are required to operate in all kinds of environment, but none poses a greater risk of wear to the engine than one rich in dust and sand. The risk is exacerbated by a situation known as *brownout*, in which a helicopter flies through the dust cloud generated by its own rotor wake when landing or taking off. This situation of brownout has received much academic attention in recent times, motivated by a desire to mitigate the loss of visual cues that can lead to spatial disorientation for the pilot (Refs. [1-4]). Additionally, in such conditions a helicopter engine working close to maximum power may ingest over a kilogram of dust with every cubic metre of air. This can cause irrevocable damage to the engine, in particular to the compressor which suffers blunted leading edges, sharpened trailing edges, reduced blade chords and increased pressure surface roughness; but also to turbine blades and combustor walls upon which finer particles deposit. Pertinently, it has been shown that particles as small as three micrometers in diameter can cause such damage [5]. These effects are highly undesirable and lead to rejections after as little as 25 hours [6], increased downtime and ultimately, cost. The effects may be mitigated somewhat by erosion resistant coating, but particles may cause damage elsewhere such as contamination of oil supplies. Therefore perhaps a more efficacious remedy is to employ a device that prevents

particulate reaching the engine from the outset. An inlet barrier filter is one such device, pictured in Fig. 1.

There are several types of particle separating device which differ in installation and subsequent performance [7]. Some extract particles by utilising inertia effects, imparting a tangential or radial change in flow direction to particulate-laden air and scavenging away particles that cannot negotiate the turn. While achieving separation to varying degrees of success, these devices require power and extract mass flow to operate. Conversely, an inlet barrier filter (IBF) separates particles more passively by arresting particles on its air-permeable surface. The device does not require power nor draw off mass flow. However, air that passes through the filter experiences a loss in total pressure, which grows temporally as particles accumulate on the surface. Hence use of these devices demands regular maintenance and constant pressure drop monitoring to ensure the benefit of protection to the engine is not outweighed by the loss to engine performance.



Fig. 1: 'Flush-type' IBF.

All IBF currently available comprise one or more filter panels resembling that which is pictured in Fig. 1. On closer inspection in Fig. 2, it is revealed that this filter panel contains a plurality of pleats of approximately three centimetres depth and one centimetre pitch. The wire mesh seen provides a level of protection to the filter against damage from sharp stones and pebbles, while retaining the multi-ply cotton fabric in a pleated formation.

As dust-laden air is drawn through the filter, particles are captured firstly within the filter medium, then on its surface. The layer of particles accumulated on the surface of a filter is commonly referred to as *cake*, and will be so too hereinafter. This two-stage process of clogging is characteristic of IBF filters and results in a bi-modal rise in pressure loss over time. The factors dictating this transient condition are numerous and must be considered in the design of IBF. One highly influential factor is the size distribution of the particles to be captured. In contrast to coarse particles, fine particles offer a high resistance when accumulating on the filter surface, but may be more dispersed within the filter resulting in a slower rate of clogging during the 'internal' stage. Symptoms such as these become important in the design of IBF; the influence of particle size is explored in the current work.

The great variation in intake types seen across the spectrum of rotorcraft designs gives rise to a number of

¹ School of MACE, George Begg Building. Corresponding Author. Email: Nicholas.Bojdo@postgrad.manchester.ac.uk

different solutions incorporating barrier filter technology. This variation arises from the engine-airframe architecture, which is dependent on the number of powerplants, the powerplant location with respect to the airframe, and the position of the engine inlet with respect to the engine itself. These must be considered in the design of IBF. On some twin-engine helicopters such as the Seaking, the powerplants lay side-by-side ahead of the rotor mast with forward-facing intakes. This may be favourable for pressure recovery during cruise, but leaves the engine rather exposed to particles and other foreign objects during near-ground operations. Conversely, smaller rotorcraft have engines typically buried somewhere behind the main rotor mast and gearbox. For such configurations intakes are located on the airframe sides, either flush with the airframe such as on the AgustaWestland AW139 or as forward facing *slots* such as on the Bell LongRanger. Pressure recovery is reduced in forward flight, but a more tangential flow direction reduces the quantity of particulate reaching the intake through the same inertial effects described above. The following work groups all such considerations together to create a framework for IBF design.



Fig. 2: Close up of IBF filter pleats.

BACKGROUND

The plethora of factors to be considered in IBF design could make establishing a design protocol a rather daunting prospect. Therefore it useful to break the problem down into scales. Four scales are identified:

1. The fibre-particle scale.
2. The pleat scale.
3. The filter panel scale.
4. The rotorcraft scale.

These are illustrated in Fig. 3. The four scales can be investigated deeper to ascertain the factors connected with filter design.

The Fibre-particle Scale

The fibre-particle scale is dealt with first. This scale is of the order 1 – 1000 micrometers. This range includes the typical filter fibre diameter of 15 micrometers, and the spectrum of typical dust diameters (from fine clay dust to coarser silica particles). Filtration at this scale has been studied in depth for many decades, but is still not fully understood. Many theories of filtration rely on empirical

data or case specific formulae to predict the *capture efficiency* (ability to retain particles) and subsequent loss in pressure of a given filter operating in a given flow. Prediction is further complicated by the bi-modal aspect of filtration and as such the two stages are often dealt with separately.

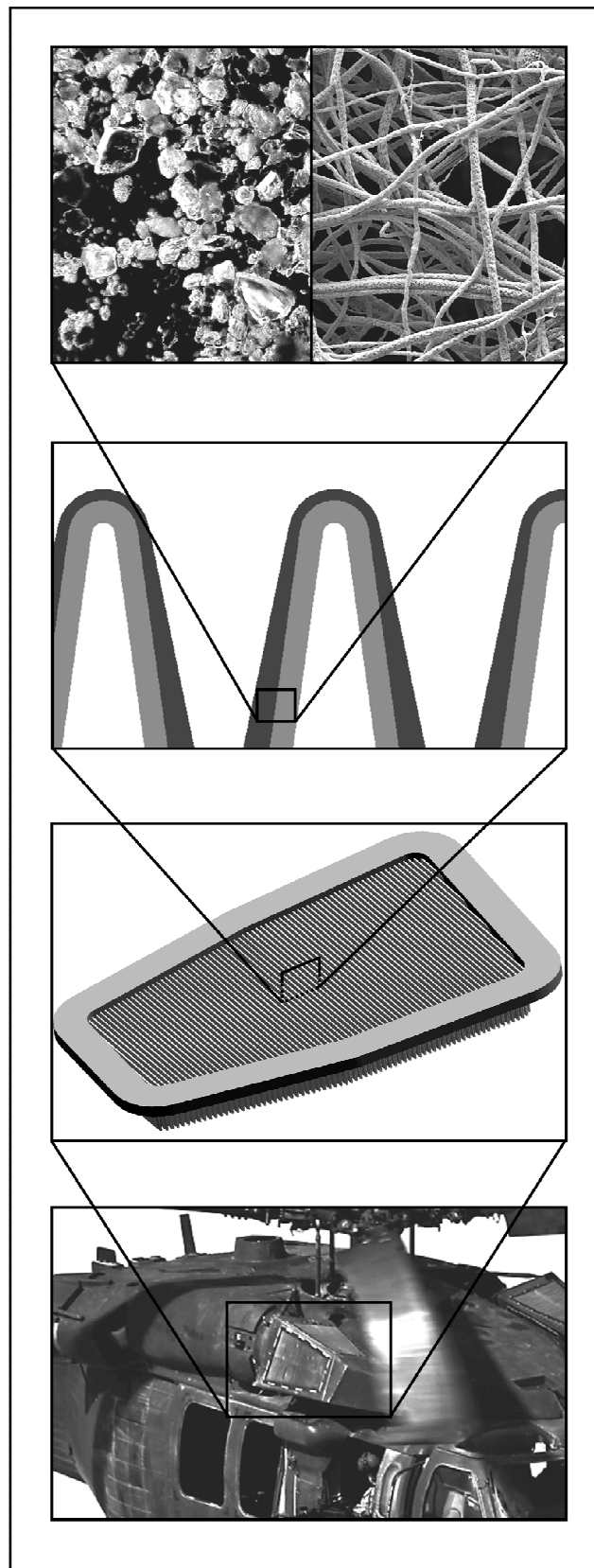


Fig. 3: The four IBF scales from top to bottom: Fibre-particle scale; Pleat scale; Filter panel scale; Rotorcraft scale. Picture references: [10-12].

These differences yield a performance which depends largely on the particle and flow properties. Increasing the number of fibres in a filter may improve the efficiency, but at the expense of pressure drop. From a design point of view, these two performance indicators can be combined to ascertain an optimum point for a given set of boundary conditions.

Theories of fibre-particle interaction are outlined in depth in the books of Davies [8] and Brown [9]. Three *capture mechanisms* are identified, the influence of which is mainly dependent on particle Reynolds number:

- i. *Diffusion*, by which particles are intercepted by fibres as they wander in random Brownian motion, crossing fluid streamlines.
- ii. *Direct Interception*, by which particles follow fluid streamlines around a fibre, but are intercepted by virtue of their bulk.
- iii. *Inertial Impaction*, by which particles possessing too much inertia cannot negotiate the flow path around the fibre and leave the streamline to deposit on the fibre surface.

These three mechanisms act collectively to give the filter an *overall capture efficiency*, which may be augmented by other factors such as electrostatic charge, van der Waals force, gravity and surface tension. The three main mechanisms vary in dominance over the particle diameter, particle velocity, fibre diameter, and filter solidity scales. Diffusion acts at the smallest scale but diminishes as the Peclet number increases beyond approximately 0.1. As the Stokes number rises above 0.2, inertial impaction increases its influence but becomes the only mechanism acting, as particles no longer follow streamlines. The characteristic deficit in efficiency between these two limits is cushioned by the interception mechanism, which is dependent on the particle radius, fibre radius, and spacing between fibres.

For the case of IBF, filter medium choice is complicated by the large range of particle sizes required to be captured. If it is assumed that one micrometer represents the smallest size of particle to be removed, then inertial impaction will be the dominant capture mechanism. Diffusion is not present, and direct interception will occur over only a small range. The current solution is a multi-ply woven fabric filter. The criticalness of this choice is unknown; however a performance improvement may be met if each layer is designed differently. For example, if a layer of lower packing fraction (no. of fibres per unit volume) is chosen as the leading layer, it will achieve good capture efficiency for large particles, utilising inertial impaction, but may permit smaller more penetrative particles through. These smaller particles can be captured later by adjacent layers that are packed more tightly with perhaps larger diameter fibres. Creating capture ‘schedules’ in this way means each layer is tuned to operate at a maximum efficiency.

Particles arrested on the surface of a filter begin to accumulate as a *surface cake*. This may occur if the particles are too big to permeate the filter pores; it may also occur if the filter medium has reached *capacity*. In this state pores have become blocked or partially blocked by previously captured particles and cannot be penetrated any longer by even the smaller dust particles. Like the overall filter efficiency, the resulting pressure drop across the cake is highly dependent on the sizes and shapes of the particles of which it is composed. While the structure of

the cake cannot be altered by design, knowledge of its behaviour can help to optimise the solution.

Theoretical derivation of pressure drop through porous matrices has been widely studied and is not yet fully understood. Models range from theoretical to empirical; sometimes a combination of the two; but most are based on the following relationship:

$$-\frac{dp}{dx} = \mu \frac{Q}{A_F} C + \frac{1}{2} \rho_g \left(\frac{Q}{A_F} \right)^2 D \quad (1)$$

Where dp/dx is the pressure gradient, μ is the fluid viscosity, ρ_g is the fluid density, Q the fluid volume flow rate and A_F is the filtration area. The coefficients C and D thus determine the pressure drop and are referred to as the *viscous resistance* term and *inertial resistance* term respectively. The inverse of the viscous resistance term is sometimes also referred to as the *coefficient of permeability* of a medium; it gives the measure of a porous medium’s ability to transmit fluid. Derivations of these coefficients are numerous, a review of which is given by Bear [13]. One such derivation is the Ergun equation, applicable to monodisperse particles of spherical shape in high volume flow. The coefficients are given as:

$$C = \frac{150(1-\varepsilon)}{\varepsilon^3 d_p^2} \quad (2)$$

$$D = \frac{3.5(1-\varepsilon)}{\varepsilon^3} \quad (3)$$

Where ε is the porosity (fraction of empty space), and d_p is the particle diameter. The coefficient C closely resembles the more commonly known Kozeny-Carman equation developed for flow at low Reynolds number, in which the quadratic term of Eq. 1 disappears.

In reality, the typical dust sample is polydisperse and contains irregular-shaped particles. Cakes composed of such particles tend to offer more resistance to flow due to smaller particles filling the voids of the larger particles’ interstices. Ergun’s equation can still be applied using the 50% mean diameter of the particle size distribution (PSD), but this has been shown to be inadequate. In his studies on a number of cake samples, Wakeman asserts that a more appropriate reference diameter would be the 5 or 10% size [14]. In a separate study, Endo *et al.* derives an expression for pressure drop based on the sum of the drag acting on all particles of a cake [15]. The drag of a single particle is given by:

$$F_1 = \frac{\pi}{8} d_v^2 \rho_g u_i^2 \left(0.55 + \frac{4.8}{\sqrt{\text{Re}_p}} \right)^2 \kappa \quad (4)$$

$$\text{Re}_p \equiv \frac{\rho_g u_i d_v}{\mu} \quad (5)$$

Where κ is the dynamic shape factor, defined as the ratio of the drag force on the particle in question to that on a sphere of the volume equivalent diameter. If the PSD obeys a log-normal distribution, the total drag can be formulated by integrating over the entire particle distribution. For full derivation see Endo *et al.* [15]. The pressure drop per unit volume of cake is:

$$\begin{aligned} \Delta P_C = F_C \frac{u_i}{u_s} H = \\ 0.2269 \rho_g u_s^2 H \frac{(1-\varepsilon)v(\varepsilon)}{\varepsilon^3} \frac{\kappa}{d_{vg} \exp\left(\frac{5}{2} \ln^2 \sigma_g\right)} \\ + 3.96 \sqrt{\rho_g \mu u_s^{1.5}} H \frac{(1-\varepsilon)v(\varepsilon)}{\varepsilon^{2.5}} \frac{\kappa}{d_{vg}^{1.5} \exp\left(\frac{27}{8} \ln^2 \sigma_g\right)} \\ + 17.28 \mu u_s H \frac{(1-\varepsilon)v(\varepsilon)}{\varepsilon^2} \frac{\kappa}{d_{vg}^2 \exp\left(4 \ln^2 \sigma_g\right)} \end{aligned} \quad (6)$$

The latter two parameters can be determined by spectral analysis of a given dust sample; the void function and shape factor can be determined experimentally.

This equation has been shown to yield accurate results for a polydisperse cake such as one composed of AC fine particles (Arizona Road Dust). With respect to IBF design, it will be seen that combined with known properties of the filter medium, the prediction of cake pressure drop allows pleat geometry to be optimised for a given target dust sample.

Pleat Scale

The next scale of IBF design is the pleat scale. The filter medium of an IBF is pleated to increase its surface area. A typical IBF pleat has a depth of around three centimetres and a pitch of around one centimetre, which increases the filtration surface area sixfold. This has two beneficial effects: first, the filtration velocity (or volume flow rate per unit area, perpendicular to the filter surface) decreases, which reduces the pressure drop in accordance with Eq. 1; second, it allows the filter to retain more particles, which improves its service life. However, pleating introduces a second source of pressure loss within the pleat gaps, which grows as the gaps become narrower or accumulate particles. This results in an optimum pleat geometry which becomes the focus of design at this scale.

Many studies have attempted to theorise the design point to eliminate the need for trial and improvement methods of optimisation. Studies initially focused on clean filters subjected to low Reynolds number flows (Refs. [16], [17]) however in the extension to IBF, several differences arise. Firstly, the anticipated volume flow rate is at least an order of magnitude greater. Secondly, as a filter accumulates particles its properties change, which alters the optimum point. The work Rebai *et al.* investigates this feature with a flow of Reynolds number similar to the current application [18]. A semi-analytical model is proposed to predict the transient pressure drop across a pleat upon which particles collect. As well as exhibiting the classic optimum design point for minimum pressure drop of a clean pleated filter, the study yielded a secondary optimum design point: a pleat number that can retain a maximum mass of particles for a given pressure drop. They found that a filter designed for optimum holding capacity (quantity of captured particulate for a given pressure drop) would favour a higher pleat number than one designed for minimum clean pressure drop, the extent of the increase being dependent on flow rate and pleat depth.

These conclusions are to be considered in IBF design. In addition to the flow rate and pleat depth, however, it is hypothesised that the optimum holding capacity alters

depending on the dust type, too. This is because the resulting filter cake behaves differently depending on its constituent particles. The current work investigates this phenomenon.

Intake Scale

A typical IBF is shown in Fig. 1. It represents one type of design solution in which the primary filter panel is blended with the original airframe, facing up towards the rotor disk. Similar solutions exist for other light rotorcraft of relatively small engine mass flow requirements (around 1 to 3 kgs⁻¹). Visible on the module side is a mandatory *bypass door*. The bypass door can be operate manually by the pilot in the event of a severely clogged or malfunctioning IBF to provide a free path for the air to reach the engine. It is another aspect of IBF integration that must be considered at the design stage. Not visible in Fig. 1 is a secondary filter panel at the front of the module. This faces forward, sat just behind the main rotor shaft and original intake.

The secondary filter panel is an example of what is termed by the authors: *plenum-type* IBF installation. In several helicopter configurations the engines are sat behind the main rotor mast, with their inlets shrouded by a nacelle. Air is drawn through forward-facing side ports into an inlet plenum. If the shape of these ports is unusual or their cross-sectional area small, the solution is to place an IBF panel within the chamber. Larger engines may require a box-like construction, as illustrated in Fig. 4.

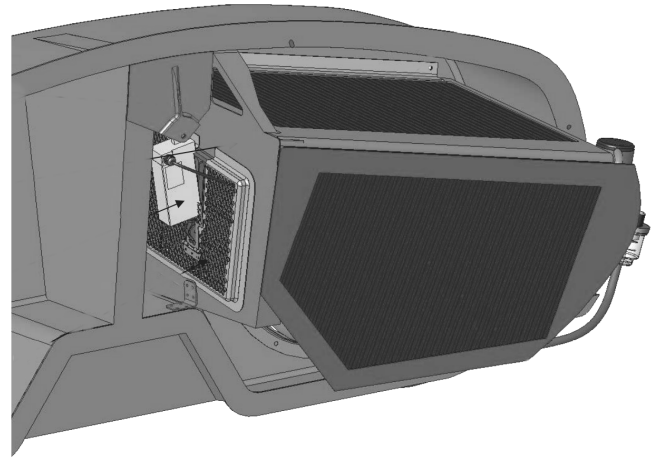


Fig. 4: Plenum-type IBF located in inlet chamber. IBF panels are shaded dark. *Image appears courtesy of AFS Donaldson [19].*

Where larger mass flow requirements are present, the IBF module is constructed as a box and attached to the front of the engine intake, in a configuration termed *exterior-type* by the authors. Substituting each side of the box for an IBF panel reduces the average throughput velocity and keeps pressure drop low. In the example shown in Fig. 5, the IBF module is connected to the intake via a duct; the bypass door resembles a small panel at the front of the module.

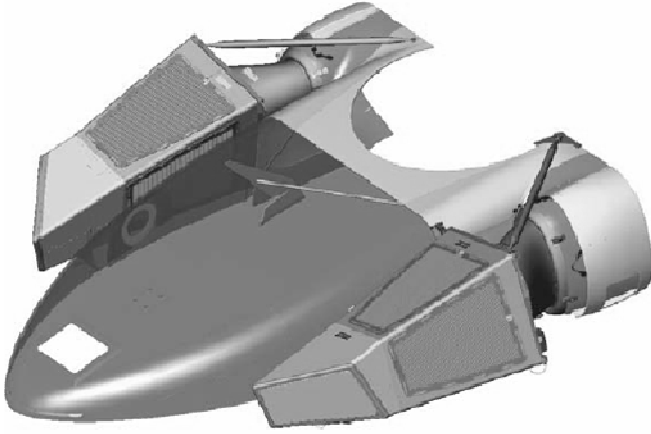


Fig. 5: Exterior-type IBF. Image appears courtesy of AFS Donaldson [19].

In summary, there is a large plethora of intake designs, which requires multiple solutions. The variation in performance of one configuration to the next is not yet known. However, design optimisation must consider additional parameters to pressure drop, holding capacity and filtration efficiency. For example, a filter panel will eventually become too clogged for suitable operation. In this event it is removed, cleaned, and re-installed; or it is replaced. For this reason the installation must permit easy access to the filter and allow panels to be detached quickly to minimise maintenance time. Furthermore, the design must incorporate a bypass door that can be manually operated by the pilot in the event of a malfunction.

Rotorcraft Scale

The rotorcraft scale concerns the rotor design parameters that contribute to the generation of the dust cloud into which the helicopter descends. There have been several studies in the last decade or so conducted with the aim of qualifying and quantifying the mechanisms of sediment uplift and particle transport in a Brownout cloud. These have been motivated by a desire to mitigate the loss of visual cues that can be troublesome to a pilot; or to simulate a brownout landing in order that a pilot may be more adequately trained to fly in such conditions. In the context of IBF design, such work may help to predict the size distribution of particles reaching the engine, and therefore aid optimisation.

Leishman and his co-workers have been studying the uplift mechanisms caused by the rotor downwash. In one study [1] they relate the uplift of particles from a sediment bed to a threshold surface wind velocity, at which the aerodynamic forces overcome the cohesive and gravitational forces acting on a particle, to lift it airborne. The particle's motion will then depend on its Stokes number: some are lifted up and away from the ground and may be re-ingested by the rotor disk; others will fall to the ground, their impact releasing more particles in a cascade process known as saltation bombardment. The velocity gradient and shear forces creating the original uplift are related to the groundwash strength, but are augmented by convecting and merging tip vortices. In a separate study [2] Leishman *et al.* relate the severity of the subsequent brownout cloud to a number of factors that can themselves be related back to rotor design parameters. Specifically, factors that appear to correlate with the development of

brownout clouds are: the average downwash velocities in the rotor wake; the blade tip vortex strengths; the total strength of the vortical wake; and the effective frequency of the impingement of the rotor wake on the ground. With further investigation it is hoped that the findings of both studies can be used in IBF design. Of particular interest are the particles that become re-ingested through the rotor disk, as it is these against which the IBF protects the engine during brownout.

PLEAT DESIGN OPTIMISATION

There are several aspects of pleat design that can be optimised. Installation can be optimised for minimum overhaul time, while the filter medium layers can be tuned to catch certain particles for a minimum pressure drop. However, one area that is most conducive to optimisation is in the geometry of the pleats. To demonstrate this, a parametric study is performed using commercial computational fluid dynamics software (CFD).

It is known that an optimum design point exists for both minimum pressure drop when the filter is clean; and maximum holding capacity when the filter is clogged. The optimum design for minimum pressure drop will depend upon, among other factors, the influent velocity magnitude. The optimum design point for maximum holding capacity will also depend upon the velocity magnitude but, as has been discussed, will be sensitive to the particle size distribution of the dust to which the filter is subjected.

Method

The latter of these is explored by subjecting a number of two-dimensional pleat designs to various flows using CFD. A typical flow domain comprises an upstream zone and a downstream zone designated as fluid, which sandwich a third zone representing the porous medium. The cells of this zone are prescribed with a time-variant momentum sink term to simulate the increasing resistance to flow posed by the filter as it becomes clogged. This is achieved by implementing a user-defined function into the boundary conditions of the porous domain. To simulate the effect of cake growth, additional zones are activated at a pre-determined time corresponding to the pleat reaching capacity. The momentum sink term is given by Eq. 1. An example domain is shown in Fig. 6. Owing to symmetry, a half-pleat need only be modelled.

For a given pleat, the rate of resistance and 'time to capacity' are dependent on the properties of the filter and the simulated mass flow of particles approaching the filter. Each pleat has identical initial properties but, owing to variations in pitch and volume, each pleat accumulates mass at different rates, and reaches capacity at different times. This can be demonstrated by considering a situation in which a filter is operating in a Brownout cloud of dust concentration c . It is assumed that the particulate-laden flow approaches the pleat parallel to the line of symmetry with magnitude U . The mass flow per unit area is given by:

$$\left(\frac{dm}{dt}\right)' = cU \quad (7)$$

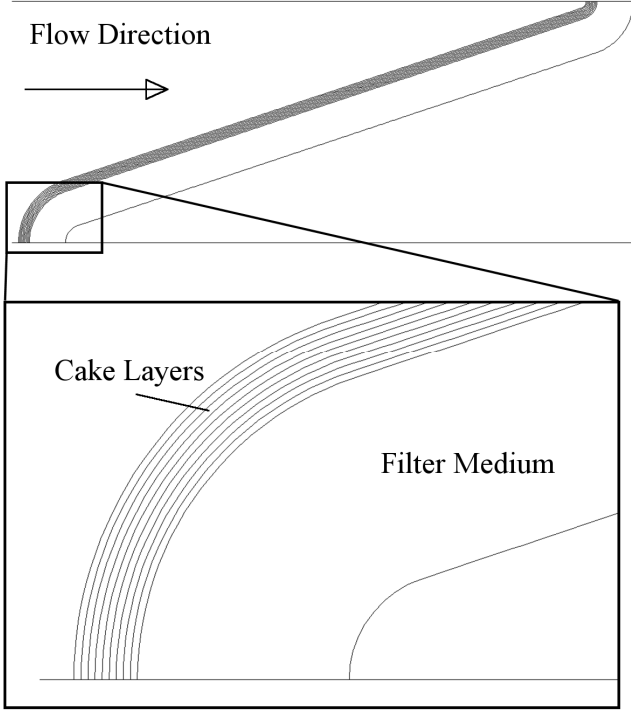


Fig. 6: Example of porous domain, showing half-pleat and cake layers.

Since working in two-dimensions, area dimensions can be given per unit length in the z -direction. Hence the mass flow of particles approaching a given half-pleat of width W_{hp} is:

$$\frac{dm}{dt} = cUW_{hp} \quad (8)$$

The capacity of a filter describes the mass of particulate that can be contained within the medium. It is assumed that each pleat design, despite being of different shape, possesses the same capacity per unit volume. The capacity can also be known as the critical mass, M_{cr} . Combining with Eq. 8, the time to capacity is thus given by:

$$T_c = \frac{M_{cr} A_{hp}}{cUW} \quad (9)$$

The time to capacity is thus unique for non-identical half-pleats. A lower half-pleat volume means capacity will be reached more quickly. Conversely a narrower pleat receives a lower mass flow rate of particulate hence clogs slower. To calculate these values in the absence of experimental data, the concentration is assumed to be that of the standard definition of Brownout, 1.177e-03 kilograms per cubic metre of particulate-laden air; and critical mass is borrowed from the work Rebai *et al.* [18] who performed a similar study for automotive applications. Concerning the latter, experiments were initially performed on a planar filter medium to ascertain its capacity. The critical mass was found to be approximately 276 kgm⁻³, when subjected to AC Fine test dust. Owing to the similarity of the present work this value was used for all pleat geometries. The values of U and W are varied as part of the parametric study.

Modelling Procedure

The objective of the present work is to demonstrate pleat design optimisation. It has been discussed that due to clogging, this is dependent on the transient conditions.

During internal clogging the filter takes on mass, which decreases its porosity thence increases its resistance to flow, as dictated by Eqs. 2 and 3. The initial porosity at time $t=0$ and fibre diameter are assumed to be that of the reference material from Rebai *et al.* [18], namely 0.9 and 14 micrometres respectively. These are substituted into Eqs. 2 and 3 to determine the initial viscous and inertial resistance terms. The contribution to resistance by collected particles is dealt with separately, with a variable porosity and diameter corresponding to the particle size of interest. However the porosity is re-written as the solidosity, or solid fraction of the filter that is made up of particles:

$$\omega_c = 1 - \varepsilon_c \quad (10)$$

Where ω_c is the cake solidosity and ε_c is the cake porosity. The rate of increase of solidosity, attributable to the collected particles is given by:

$$\frac{d\omega}{dt} = \frac{dm}{dt} \frac{1}{\rho_p A_{hp}} \quad (11)$$

Integrating Eq. 11 and substituting for ε as Eq. 10 into Eq. 2 and 3, yields the temporal viscous and inertial terms respectively, and then added to the initial coefficients for the clean filter. At time $t=T_c$, the porosity rate becomes zero and the filter porosity is held constant. This signifies that the half-pleat is full.

Modelling cake growth is slightly different. Unlike the filter medium, the temporal resistance arises not from a change in porosity but from a change in porous matrix thickness. The porosity may change due to compression of the filter cake, but due to a multitude of other factors that may affect cake structure that are not modelled here (such as humidity, cake breakdown due to vibration) this is neglected. An ideal situation is modelled, in which the cake develops evenly across the filter surface. It is comprised of monodisperse, spherical particles, the diameters of which are varied as part of the parametric study. To avoid the complications of re-meshing a moving boundary (that would represent the growing cake layer surface), a maximum cake thickness is discretised into layers. Each layer becomes 'active' when enough mass has accumulated to create its neighbouring layer. To achieve a smoother temporal variation in resistance, the cake resistance terms from Eq. 2 and 3 are modified to include a time dimension, based on the simple Euler method of interpolation. The time taken for one layer to form is given as:

$$T_l = \frac{\rho_p S_{hp} (1 - \varepsilon_c) \Delta x}{cUWA_{hp}} \quad (12)$$

Where S_{hp} is the half-pleat volume per unit length per unit thickness (or pleat front curve length), and Δx is the cake thickness. The first layer forms when the filter reaches capacity at time $t=T_c$; the next is activated at time $t=T_c+T_l$; the n th at time $t=T_c+(n-1)T_l$.

Modelling Assumptions

The following assumptions adopted in the present work are provided in summary:

- The properties of the filter medium, including its capacity and initial resistance coefficients, are taken from the study of Rebai *et al.* [18] in which the application is automotive filters.
- All particles that comprise a size group are considered monodisperse and of spherical shape.

- Particles accumulate evenly across the surface of the filter, creating a homogeneous cake of constant surface-wise thickness.

Computational Procedure

The simulations were run using commercial CFD software. Each domain varied in grid size depending on the half-pleat pitch. The smallest domain contained 30003 cells; the largest contained 85060 cells. The Reynolds Stress Model was used to solve the Reynolds-Averaged Navier Stokes equations. The fluid was prescribed with a Turbulence Intensity of 2% based on a lengthscale of 7% of channel width. Turbulence was held constant, but parts of the domain had time-dependent momentum sink terms, prescribed by user-defined functions.

Boundary Conditions and Geometry Size

The inlet velocity was 10 ms^{-1} for each pleat, and the inlet conditions were set to Standard Day, static sea level. Each pleat had a thickness of $1.5\text{e-}03 \text{ m}$. The thickness of one cake layer was $0.5 \text{ E-}03 \text{ m}$, and depth of each pleat $25\text{e-}03 \text{ m}$.

Results

The results for the four particle diameters are given in Fig. 7. The abscissa of each plot denotes number of pleats per metre span. As a reference, the filter panel in Fig. 1 has a pleat density of around 100 pleats per metre. Each plot displays two trendlines: the left ordinate denotes clean filter pressure drop; the right ordinate denotes collected mass per square metre of IBF projected area (note: not 'per square metre of filter surface area'). Concerning the latter, a pressure drop at which to take a 'mass collected' reading was chosen by considering the realistic situation. It is known from conversations with the manufacturer that the maximum pressure drop to be tolerated by a given IBF (before the performance loss is considered too great) is around 10 inches water gauge, or 3000 Pa. To establish the mass collected by a given pleat, the time elapsed as recorded per time step is multiplied by the respective mass flow rate. The point at which the associated pressure drop breaches 3000 Pa is then recorded. This routine is followed for each pleat in each scenario.

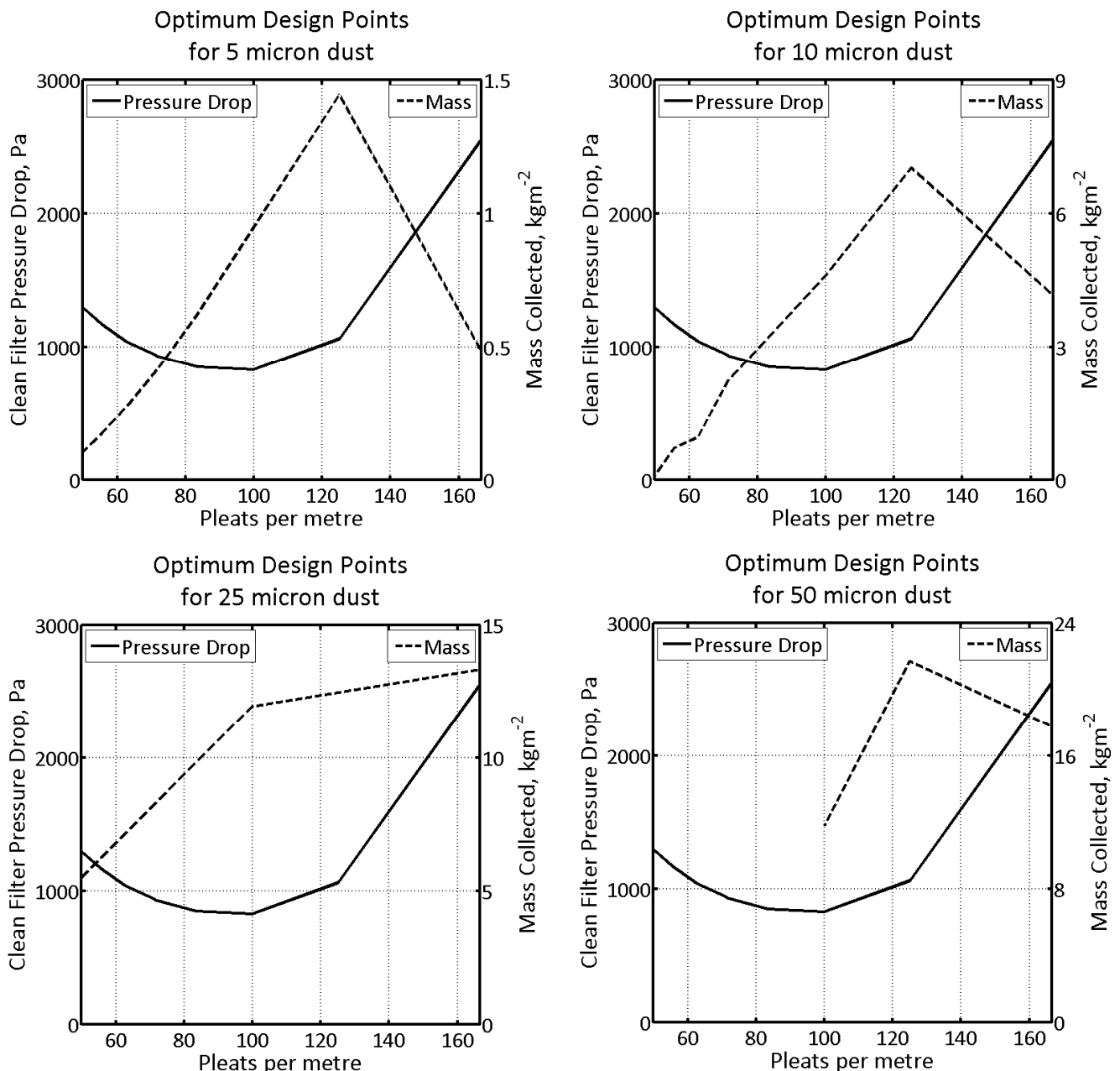


Fig. 7: Plots of clean filter pressure drop and collected mass per unit panel area of IBF, for four mean dust particle sizes.

Discussion

Analysing the results, there are certain features of note. Firstly, the characteristic U-shape pressure drop of the clean, unclogged filter is evident. Thus for a filter of thickness 1.5 millimetres in a flow of magnitude 10 ms^{-1} , the optimum design is around 85 pleats per metre. Secondly, the characteristic peak in collected mass for a given pressure drop is also evident. This occurs at the same point for all particle diameters, at around 100 pleats per metre. Thirdly, the mass of particulate that can be held by a given pleat design, increases with increasing particle diameter. For example the maximum mass of 10 micrometre dust that can be retained, before a pressure drop of 3000 Pa is reached, is 7 kgm^{-2} . This is compared to a mass of around 22 kgm^{-2} when the particle size is 50 micrometres.

The characteristic U-shape of the clean filter pressure drop and the peak in the collected mass occur due to conflicting effects of pleating. The additional surface area provided by pleating reduces the throughput filtration velocity and yields more space for capture. However pleat crowding and cake growth in narrow pleat channels introduces a second source of pressure loss through flow contraction, velocity gradients and subsequent loss flow shear stress. However, the optimum design points are different. A filter optimised to collect more mass should be designed with approximately 50% more pleats than one designed for optimum clean pressure drop.

The benefit to a filter that can retain more mass is a longer service life. Therefore designers may wish to sacrifice a higher initial pressure drop in order to increase the time between overhaul. An interesting extension to the current work would be to find the best design point between the two optimum points presented here. This may include other factors such as loss of useful power or additional fuel burn required as a result of the clogging filter's presence, and the cost of cleaning or replacing the clogged filter per overhaul. The current work ties into both areas.

One feature of the results that does not support the anticipated outcome is that each optimum pleat number for maximum collected mass occurs at the same point, irrespective of the particle diameter. This may be due to a lack of data, but clearly in this example the optimum point is not so sensitive to particle diameter. However, it is to be remembered that the sample here is a monodisperse distribution of spherical particles. A more thorough investigation of dust sands with variable porosities and log-normal distributions of particle sizes should be carried out before a conclusion is made.

DESIGN PROTOCOL

Drawing all point discussed thus far together, the work is concluded with the proposition of a design protocol. This is aided by the diagram in Fig. 8. Three main constraints are identified:

1. Particle Size Distribution (PSD).
2. Engine Mass Flow rate.
3. Intake Architecture.

The design variables that can be optimised, and that dictate the subsequent performance of the IBF are also identified. The filter can be optimised for a number of performance parameters. Concerning the installed operation of the filter, the performance is indicated by the pressure drop, holding capacity and collection efficiency. Concerning the overall

working life of the filter, performance is assessed by the ease of installation and maintenance, and the time between overhaul.

The Particle Size Distribution relates to the size range of particles in a given sample. The properties of a cake formed of such a range are dependent on the volume mean diameter and standard deviation of the sample. Since filter efficiency and filter transient pressure drop are dependent on the particle properties, design of IBF should begin by ascertaining a target particle size distribution. This may be obtained by taking a sample from a rotorcraft airframe operating in the specific environment, or may be estimated analytically through studies of the Brownout cloud. With knowledge of the particle size and standard deviation, the number of different filter layers can be set for maximum efficiency; and the number of pleats set for maximum particle retention.

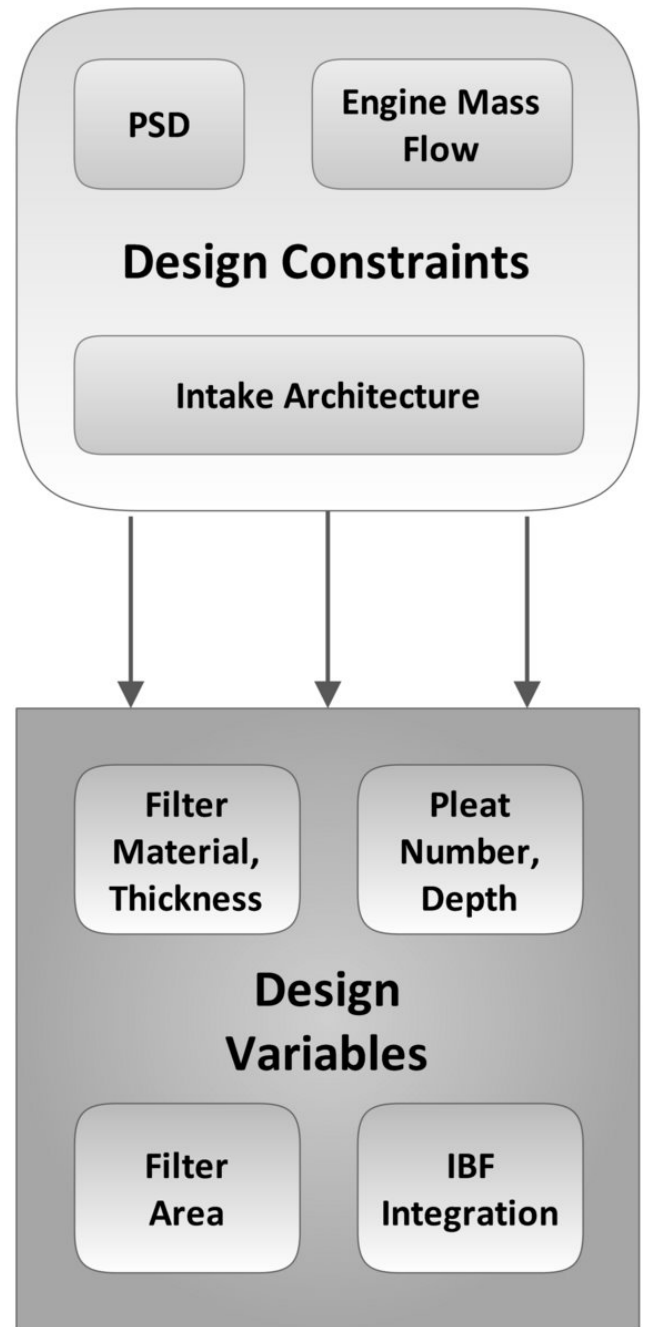


Fig. 8: IBF Design Optimisation Flowchart

The Engine Mass Flow rate determines the volume flow rate required by the engine (at a given density altitude). The collective surface area of all filter panels (if more than one) determines the flow velocity magnitude approaching the panel surface. The subsequent filtration velocity is determined by the pleat number, which can be optimised as discussed. However if the IBF projected area decreases, the approach velocity increases which may alter the optimum design point. It is known that for this reason, manufacturers of IBF aim to keep a constant panel area to achieve a flow rate of around $10 \text{ ms}^{-1}\text{m}^{-2}$. Hence with knowledge of the engine mass flow rate, the total required projected surface area of panels can be established.

The Intake Architecture is highly variable. For this reason a number of innovations exist. For a large projected area (as dictated by engine mass flow), a multiplicity of panels may be required. In this case, the IBF can be designed as a box-like structure and affixed to the front of an intake, with ducting to the engine inlet. However, where possible, such external features should be kept to a minimum to reduce drag losses. If the inlet is located in a plenum, the total surface area may be achieved with an internal multi-faceted IBF. Each panel may be curved in a direction perpendicular to the pleat line of symmetry. If the mass flow requirements are small and the factory airframe intake simple, the IBF may be blended seamlessly with the airframe. This design is preferred as it would suffer the least additional profile drag. Additionally, a performance benefit can be met if the filter can be blended into the side of a rotorcraft where the oncoming flow is generally parallel to the plane of the filter panel, as heavier particles would fail to reach the filter owing to their inertia. Finally the filter must be installed with ease-of-access considered. Throughout its life, the filter should be able to perform multiple cycles. After each cycle, it should be a straightforward process to remove the filter from the airframe, dust it off, clean it, and replace it within the time-frame constraints of a normal scheduled maintenance.

CONCLUSIONS

The work presented here ultimately aims to provide a framework for the design of Inlet Barrier Filters for rotorcraft. It also provides an overview of the relevant contributory factors to IBF design and describes the key compromises in optimisation.

Optimisation occurs at almost all scales of IBF design, of which there are four: the fibre-particle scale, the pleat scale, the intake scale and the rotorcraft. The fibre-particle scales focuses on the structure of the porous matrix, which comprises the filter medium – randomly assorted nano-fibres or woven cotton yarns – and the filter cake. The filter medium structure can be tuned to capture a particular particle size, but any changes to increase capture efficiency must be made with the pressure drop in mind. Similarly at the pleat scale there exists an optimum number of pleats per metre for which a minimum pressure drop in a given flow can be achieved, when the filter is clean. However the service life of the filter can be extended by increasing this number by 50%. A balance between the two must be met. At the intake scale, the compromise is between required panel surface area and ease of integration. The greater the required surface area, the bigger the IBF, the greater the challenge to fit the intake architecture with a seamless module.

Thus there are three constraints by which to design an IBF for rotorcraft: the Particle Size Distribution of the operational environment; the Engine Mass Flow rate; and the Intake Architecture. The first sets the design of the filter medium and the optimum pleat shape for maximum holding capacity; the second sets the required total IBF panel area for a given target volume flow rate per unit area; the third governs the type of IBF to be designed. A Design Protocol proposed in the present work should, if followed, yield an optimum IBF design.

NOMENCLATURE

A_{hp}	half-pleat volume per unit length, m^3m^{-1}
C	viscous resistance coefficient, m^2
D	inertial resistance coefficient
F_c	drag on whole cake, N
F_l	drag on a single particle, N
H	cake height, m
M_{cr}	mass at filter capacity, kg
Q	volume flow rate, m^3s^{-1}
Re_p	particle Reynolds number
ΔP_c	cake pressure drop, Pa
S_{hp}	half-pleat volume per unit length per unit thickness $\text{m}^3\text{m}^{-1}\text{m}^{-1}$
T_c	time to filter capacity, s
T_l	time to cake layer growth, s
U	inlet velocity, ms^{-1}
W_{hp}	half-pleat width, m
c	particulate mass concentration, kgm^{-3}
d_p	particle diameter, m
d_v	volume equivalent diameter, m
d_{vg}	geometric mean diameter, m
dp/dx	pressure gradient across filter, Pam^{-1}
dm/dt	mass flow rate, kgs^{-1}
$(dm/dt)'$	mass flow per unit area, $\text{kgs}^{-1}\text{m}^{-2}$
u_i	interstitial velocity, ms^{-1}
u_s	superficial velocity, ms^{-1}
ε	porosity
ε_c	cake porosity
κ	dynamic shape factor
μ	dynamic viscosity, $\text{kgm}^{-1}\text{s}^{-1}$
ρ_g	air density, kgm^{-3}
ρ_p	particle density, kgm^{-3}
σ_g	geometric standard deviation
$v(\varepsilon)$	cake void fraction
ω_c	cake solidosity

REFERENCES

- [1] J. Leishman, "Investigation of Sediment Entrainment in Brownout Using High-Speed Particle Image Velocimetry," in *Proceedings of the 65th Annual American Helicopter Society Forum*, May 2009.
- [2] J. Milluzzo and G. Leishman, "Assessment of Rotorcraft Brownout Severity in Terms of Rotor Design Parameters," *Journal of the American Helicopter Society*, vol. 55 (3), pp. 032009–1, 2010.
- [3] C. Phillips and R. E. Brown, "Eulerian simulation of the fluid dynamics of helicopter brownout," in *Proceedings of the 64th American Helicopter Society Annual Forum*, May 2008.

- [4] C. Phillips, H. W. Kim, and R. E. Brown, "Helicopter brownout - Can it be modelled?," *Aeronautical Journal*, vol. **115** (1164), pp. 123-133, 2011.
- [5] J. P. V. D. Van Der Walt and A. Nurick, "Erosion of Dust-Filtered Helicopter Turbine Engines Part I: Basic Theoretical Considerations," *Journal of Aircraft*, vol. **32** (1), pp. 106-111, Jan. 1995.
- [6] P. Stallard, "Helicopter Engine Protection," *Perfusion*, vol. **1997** (12), pp. 263 - 267, Jul. 1997.
- [7] A. Filippone and N. Bojdo, "Turboshaft engine air particle separation," *Progress in Aerospace Sciences*, vol. **46** (5), pp. 224-245, July 2010.
- [8] C. N. Davies, *Air Filtration*. Academic Press, 1973.
- [9] R. C. Brown, *Air Filtration: An Integrated Approach to the Theory and Applications of Fibrous Filters*. Pergamon Press, 1993.
- [10] BASF - The Chemical Company, *A whiff of nothing*. Jan. 2010. [Photograph]
- [11] I. Russell, *Icelandic volcanic ash over Britain 1*. Apr. 2010. [Photograph]
- [12] The U.S. Army, *A day with Black Hawk crews*. Aug. 2008. [Photograph]
- [13] J. Bear, *Dynamics of Fluids in Porous Media*, 1st ed. Elsevier, 1972.
- [14] R. Wakeman, "The influence of particle properties on filtration," *Separation and Purification Technology*, vol. **58** (2), pp. 234-241, Dec. 2007.
- [15] Y. Endo, D.-R. Chen, and D. Y. H. Pui, "Effects of particle polydispersity and shape factor during dust cake loading on air filters," *Powder Technology*, vol. **98** (3), pp. 241-249, Aug. 1998.
- [16] D. Y. H. Pui Da-Ren Chen and B. Y. H. Liu, "Optimization of pleated filter design using a finite-element numerical method," *Journal of Aerosol Science*, vol. **24** (1), p. S39-S40, 1993.
- [17] T. Lücke and H. Fissan, "The prediction of filtration performance of high efficiency gas filter elements," *Chemical Engineering Science*, vol. **51** (8), pp. 1199-1208, Apr. 1996.
- [18] M. Rebai, M. Prat, M. Meireles, P. Schmitz, and R. Baclet, "Clogging modeling in pleated filters for gas filtration," *Chemical Engineering Research and Design*, vol. **88** (4), pp. 476-486, Apr. 2010.
- [19] "Aerospace Filtration Systems (AFS)." [Online]. Available: <http://afs.donaldson.com/>. [Accessed: 28-Jun-2011].